Inorganic Chemistry
Article

Inorg. Chem. **2009**, *48*, 7251–7260 **7251**
DOI: 10.1021/ic9005899

Magnetic and Spectroscopic Properties of Mixed Valence Manganese(III,IV) Dimers: A Systematic Study Using Broken Symmetry Density Functional Theory

Maylis Orio, Dimitrios A. Pantazis, Taras Petrenko, and Frank Neese*

Lehrstuhl für Theoretische Chemie, Institut für Physikalische und Theoretische Chemie, Universität Bonn, Wegelerstrasse 12, D-53115 Bonn, Germany, and Max-Planck-Institut für Bioanorganische Chemie, Stiftstrasse 34-36, D-45470 Mülheim an der Ruhr, Germany

Received March 26, 2009

Exchange coupling parameters and isotropic ^{55}Mn hyperfine couplings of fourteen mixed-valence Mn(III)−Mn(IV) dimers are determined using broken-symmetry density functional theory (DFT) and spin projection techniques. A systematic evaluation of density functional approaches shows that the TPSSh functional yields the best exchange coupling constants among all investigated methods, with deviations from experiment of the order of ∼10−15%. For the prediction of ^{55}Mn hyperfine couplings the deficiencies of DFT in the description of core-level spin-polarization and the neglect of scalar relativistic effects lead to systematic deviations between theory and experiment that can be compensated through the use of a universal scaling factor. We determine this scaling factor to be 1.49 and demonstrate that the ^{55}Mn hyperfine couplings in mixed-valence Mn(III,IV) dimers can be successfully and systematically predicted with the TPSSh functional and the proposed spin projection techniques. The dependence of isotropic ^{55}Mn hyperfine couplings on the Mn(III) zero-field splitting values is studied in detail using a dimer for which the strong exchange approximation breaks down. In this case we apply a rigorous form of our spin projection technique that incorporates zero-field splitting contributions to the site spin expectation values. These results form the basis for future studies that aim at deducing unknown structures on the basis of computed spectroscopic parameters.

Introduction

Manganese clusters with magnetically interacting open-shell ions feature prominently in diverse areas of modern chemistry. The exchange interactions between paramagnetic Mn centers lead to intriguing properties that justify the central position these clusters occupy in research fields ranging from biochemistry to molecular magnetism. Mixed-valence manganese dimers have been extensively researched because they are the building blocks of more complex inorganic or biological systems, and they offer the opportunity to probe fundamental properties in the simplest possible chemical framework. Thus, they are the stepping stone for a deeper understanding of biological systems like the tetranuclear Oxygen Evolving Complex (OEC) in Photosystem II or the active site of Mn catalases, and they form the basis for establishing and evaluating theoretical protocols that can be subsequently extended to larger systems.[1−4] Many dinuclear complexes have been synthesized and studied over the years and of particular interest are those that mimic structural, spectroscopic, and/or functional properties of enzymes.[1−6] Modeling these properties using quantum chemical methods allows a direct connection between structure and properties to be established, and thus is a fundamental prerequisite for rationalizing observations, making predictions, and planning future research.

A direct approach to the theoretical description of exchange-coupled metal clusters requires multideterminantal methods. However, the high computational effort involved imposes strict limits to the applicability of these methods. The use of density functional theory (DFT)[7−9] in its broken-symmetry (BS) implementation[10−12] offers a way to circumvent this issue. Numerous studies have shown that the BS-DFT approach can provide reasonably good geometries

*To whom correspondence should be addressed. E-mail: neese@thch.uni-bonn.de.

(1) Mukhopadhyay, S.; Mandal, S. K.; Bhaduri, S.; Armstrong, W. H. *Chem. Rev.* **2004**, *104*, 3981–4026.
(2) Mullins, C. S.; Pecoraro, V. L. *Coord. Chem. Rev.* **2008**, *252*, 416–443.
(3) Dismukes, G. C. *Chem. Rev.* **1996**, *96*, 2909–2926.
(4) Wu, A. J.; Penner-Hahn, J. E.; Pecoraro, V. L. *Chem. Rev.* **2004**, *104*, 903–938.
(5) Manchanda, R.; Brudvig, G. W.; Crabtree, R. H. *Coord. Chem. Rev.* **1995**, *144*, 1–38.
(6) Wieghardt, K. *Angew. Chem., Int. Ed. Engl.* **1989**, *28*, 1153–1172.
(7) Parr, R. G.; Yang, W. *Density-Functional Theory of Atoms and Molecules*; Oxford University Press: Oxford, 1989.
(8) Koch, W.; Holthausen, M. C. *A Chemist's Guide to Density Functional Theory*; 2nd ed.; Wiley-VCH: Weinheim, 2001.
(9) Orio, M.; Pantazis, D. A.; Neese, F. *Photosynth. Res.* **2009**, DOI: 10.1007/s11120-009-9404-8.
(10) Noodleman, L. *J. Chem. Phys.* **1981**, *74*, 5737–5743.
(11) Noodleman, L.; Case, D. A. *Adv. Inorg. Chem.* **1992**, *38*, 423–470.
(12) Noodleman, L.; Davidson, E. R. *Chem. Phys.* **1986**, *109*, 131–143.

Published on Web 07/08/2009

and energies, while the methodology can also be applied to the calculation of molecular properties.[13−18] As a prominent example, the use of procedures based on the Spin Hamiltonian (SH) formalism in combination with appropriate spin projection allows the accurate prediction of magnetic and spectroscopic parameters like exchange coupling constants, hyperfine coupling constants, or g-tensors.[19−23]

In this paper we will follow this approach to probe the magnetic and spectroscopic properties of a series of mixed-valence Mn(III,IV) dimers. Particular emphasis is placed on the correct prediction of hyperfine coupling constants, since these form an invaluable set of experimental data in the field of OEC research.[24,25] We will show that an approach based on BS-DFT calculations combined with the determination of proper exchange coupling constants and on-site spin coefficients provides a reliable way to predict the properties of these dimers.

Among the multitude of dinuclear complexes that have been structurally characterized, several bridging modes tend to appear repeatedly.[1] The simplest dinuclear structures utilize a single oxo or hydroxo ligand. This bridging type is not often encountered because dioxo- and dihydroxo-bridged manganese dimers tend to be thermodynamically more stable than their single oxo- and hydroxo-bridged counterparts. The single μ-oxo bridge is also less common than the μ-hydroxo or μ-alkoxo motifs and is correlated with linear Mn−O−Mn geometries. A multitude of bis(μ-oxo) dimanganese clusters have been synthesized and are the most prevalent dimeric form of manganese in the literature. The less common bis(μ-hydroxo) and bis(μ-alkoxo) equivalents display remarkable similarities in core structure with the bis(μ-oxo) clusters even though they have quite different chemical environments. In the case of the bis(μ-oxo) core, the dimers typically present high oxidation states (III,IV or IV,IV) and the mixed valence clusters display valence localization. The second most common type of core is the bis(μ-oxo)(μ-carboxylato). This and the bis(μ-oxo) core are two of the bridging types that are generally accepted to occur in the OEC.[26−29] Triply bridged (μ-oxo)bis(μ-carboxylato) Mn dimers have been characterized and several interesting models exist that exhibit more than one mode of carboxylate binding to the metal center. After surveying the existing literature, we have compiled a set of fourteen mixed-valence Mn(III/IV) complexes (see Table 1) that will be studied in the present paper. Since our focus is on the correct prediction of both magnetic and spectroscopic properties, the criterion for this selection was the availability of both exchange coupling and hyperfine parameters for unambiguously characterized molecular structures. The compiled set contains all existing Mn(III,IV) dimers for which reliable data on both types of properties are available.

Methodological Details

Theoretical Methods. The interpretation of hyperfine coupling constants (HFCs) is based on the familiar Spin-Hamiltonian (SH) $H = \hat{S}\cdot\tilde{A}\cdot\hat{I}$, where $\hat{I}$ is the nuclear spin operator, $\tilde{A}$ the hyperfine coupling tensor, and $\hat{S}$ the operator of the fictitious ground-state electron spin. In the present case, the complexes of interest consist of two antiferromagnetically coupled manganese centers and are experimentally characterized as having doublet ground states (total spin $S_t = {}^1/_2$). Such coupled states can be described reasonably well by the broken symmetry (BS) approach,[10,12] as already demonstrated in studies of related systems.[21,30] It is well-established that the electron density of the relevant BS state corresponds well to the electron density of the real antiferromagnetic state owing to the variational adjustment of the ionic and neutral components of the wave function, even though the spin density is incorrect.[13,31] In a recent contribution we have successfully set up a general procedure for extracting the correct HFCs from a BS-DFT calculation of exchange coupled oligonuclear complexes, allowing the direct comparison of computed and experimentally determined HFC values.[19] For that purpose, we used a set of pairwise exchange couplings and exact diagonalization of the associated SH matrix to calculate site-spin expectation values for each magnetic center. Through the definition of appropriate spin-projection coefficients we then arrive at effective isotropic and anisotropic HFCs. The method has been discussed extensively for the general case,[19] so we will now offer only a brief outline.

By defining the system under investigation as consisting of metal-centered subsystems with definite properties and assuming that nucleus K belongs to subsystem A, we obtain the general equation that directly connects the BS calculation to the observable HFC:

$$A_{iso}^{(K)} = A_{iso,site}^{(K)}\left(\frac{\langle S_z^{(A)}\rangle}{S_t}\right) \quad (1)$$

where S_t is the fictitious total spin employed in the analysis ($^1/_2$ in our case), $\langle S_Z^{(A)}\rangle$ is the on-site spin expectation value, and $A_{iso,site}^{(K)}$ is the intrinsic site isotropic hyperfine coupling constant

$$A_{iso,site}^{(K)} = \pm A_{iso,BS}^{(K)}\left(\frac{\langle S_z\rangle_{BS}}{S_A}\right) \quad (2)$$

where S_A is the "site-spin" of subsystem A, and the positive or negative sign is applied depending on whether that fragment carries majority (α) or minority (β) spin. $\langle S_z\rangle_{BS} = M_{S_t}$ is simply the total M_S of the BS wave function and $A_{iso,BS}^{(K)}$ the calculated BS hyperfine coupling constant. Note that the on-site spin expectation value $\langle S_z^{(A)}\rangle$ is the key for arriving at the correct HFCs. In the general formulation of our procedure we consider the system of interest as divided into N subsystems

(13) Neese, F. *Coord. Chem. Rev.* **2009**, *253*, 526–563.
(14) Ciofini, I.; Daul, C. A. *Coord. Chem. Rev.* **2003**, *238−239*, 187–209.
(15) Neese, F. *J. Biol. Inorg. Chem.* **2006**, *11*, 702–711.
(16) Ruiz, E. *Struct. Bonding (Berlin)* **2004**, *113*, 91–102.
(17) Ruiz, E.; Cano, J.; Alvarez, S.; Alemany, P. *J. Comput. Chem.* **1999**, *20*, 1391–1400.
(18) McGrady, J. E.; Stranger, R. *J. Am. Chem. Soc.* **1997**, *119*, 8512–8522.
(19) Pantazis, D. A.; Orio, M.; Petrenko, T.; Zein, S.; Bill, E.; Lubitz, W.; Messinger, J.; Neese, F. *Chem.−Eur. J.* **2009**, *15*, 5108–5123.
(20) Kossmann, S.; Kirchner, B.; Neese, F. *Mol. Phys.* **2007**, *105*, 2049–2071.
(21) Sinnecker, S.; Neese, F.; Noodleman, L.; Lubitz, W. *J. Am. Chem. Soc.* **2004**, *126*, 2613–2622.
(22) Neese, F. *Inorg. Chim. Acta* **2002**, *337C*, 181–192.
(23) Kaupp, M.; Bühl, M.; Malkin, V. G. *Calculation of NMR and EPR Parameters: Theory and Applications*; Wiley-VCH: Weinheim, Germany, 2004.
(24) Kulik, L. V.; Epel, B.; Lubitz, W.; Messinger, J. *J. Am. Chem. Soc.* **2007**, *129*, 13421–13435.
(25) Kulik, L. V.; Epel, B.; Lubitz, W.; Messinger, J. *J. Am. Chem. Soc.* **2005**, *127*, 2392–2393.
(26) Yano, J.; Yachandra, V. K. *Inorg. Chem.* **2008**, *47*, 1711–1726.
(27) Kern, J.; Biesiadka, J.; Loll, B.; Saenger, W.; Zouni, A. *Photosynth. Res.* **2007**, *92*, 389–405.
(28) Yano, J.; Kern, J.; Sauer, K.; Latimer, M. J.; Pushkar, Y.; Biesiadka, J.; Loll, B.; Saenger, W.; Messinger, J.; Zouni, A.; Yachandra, V. K. *Science* **2006**, *314*, 821–825.
(29) Lundberg, M.; Siegbahn, P. E. M. *Phys. Chem. Chem. Phys.* **2004**, *6*, 4772–4780.
(30) Sinnecker, S.; Neese, F.; Lubitz, W. *J. Biol. Inorg. Chem.* **2005**, *10*, 231–238.
(31) Neese, F. *J. Phys. Chem. Solids* **2004**, *65*, 781–785.

Table 1. Mixed-Valence Manganese(III/IV) Complexes Included in the Present Study

label	compound[a]	references
1	$[Mn_2(\mu\text{-}O)(bpmsed)_2]^{3+}$	53
2	$[Mn_2(\mu\text{-}O)_2(bpy)_4]^{3+}$	57,58
3	$[Mn_2(\mu\text{-}O)_2(phen)_4]^{3+}$	58,59
4	$[Mn_2(\mu\text{-}O)_2(bispiMe_2en)_2]^{3+}$	60
5	$[Mn_2(\mu\text{-}O)_2(bisimMe_2en)_2]^{3+}$	61
6	$[Mn_2(\mu\text{-}O)_2(bispicen)_2]^{3+}$	62,63
7	$[Mn_2(\mu\text{-}O)_2(tren)_2]^{3+}$	62,64
8	$[Mn_2(\mu\text{-}O)_2(bpg)_2]^{+}$	65
9	$[Mn_2(\mu\text{-}O)_2(\mu\text{-}OAc)(dtne)]^{2+}$	58
10	$[Mn_2(\mu\text{-}O)_2(\mu\text{-}OAc)(Me_4dtne)]^{2+}$	58
11	$[Mn_2(\mu\text{-}O)_2(\mu\text{-}OAc)(tacn)_2]^{2+}$	58,66
12	$[Mn_2(\mu\text{-}O)_2(\mu\text{-}OAc)(tpen)]^{2+}$	67
13	$[Mn_2(\mu\text{-}O)_2(\mu\text{-}OAc)(bpea)_2]^{2+}$	68
14	$[Mn_2(hCl_2salpn)_2(THF)]^{+}$	55,69

[a] Ligand abbreviations: bpmsed = *N,N*-bis(2-pyridylmethyl)-*N*′-salicylidene-1,2-diaminoethane; bpy = 2,2′-bipyridyl; phen = 1,10-phenanthroline; bispiMe$_2$en = *N,N*′-dimethyl-*N,N*′-bis(2-pyridylmethyl)-1,2-diaminoethane; bisimMe$_2$en = *N,N*′-dimethyl-*N,N*′-bis(imidazol-4-ylmethyl))-1,2-diaminoethane; bispicen = *N,N*-bis(2-pyridylmethyl)-1,2-diaminoethane; tren = tris-(2-aminoethyl)amine; bpg = *N,N*-bis(2-pyridylmethyl)glycinate; dtne = 1,2-bis(1,4,7-triazacyclonon-1-yl)ethane; Me$_4$dtne = 1,2-bis(4,7-dimethyl-1,4,7-triazacyclonon-1-yl)ethane; tacn = 1,4,7-triazacyclononane; tpen = *N,N,N*′,*N*′-tetrakis(2-pyridylmethyl)-1,2-diaminoethane; bpea = *N,N*-bis(2-pyridylmethyl)ethylamine; hCl$_2$salpn = *N,N*′-bis(3,5-dichlorosalicylidene)-1,3-diamino-2-hydroxypropane; THF = tetrahydrofuran.

interacting via $N(N-1)/2$ Heisenberg exchange couplings corresponding to the effective spin-Hamiltonian of eq 3.

$$H_{\text{eff}} = -2\sum_{i<j} J_{ij}\hat{S}_i\cdot\hat{S}_j \tag{3}$$

The eigenstates of H_{eff} are

$$|S_A S_B ... S_{N-1} S_N SM\rangle = \sum_{S_A M_{S_A} ... S_N M_{S_N}} C_I^{S_A M_{S_A} ... S_N M_{S_N}} |S_A M_{S_A}, ..., S_N M_{S_N}\rangle \tag{4}$$

and for a given subsystem A, the on-site spin expectation value is calculated as

$$\langle S_z^{(A)}\rangle = \sum_{S_A M_{S_A} ... S_N M_{S_N}} |C_I^{S_A M_{S_A} ... S_N M_{S_N}}|^2 M_{S_A} \tag{5}$$

where $|C_I^{S_A} M_{SA},...,S_N M_{SN}|^2$ represents the weight of the basis state $|S_A M_{SA},...,S_N M_{SN}\rangle$ in the ground state eigenfunction $|S_A S_B ... S_{N-1} SM\rangle$ with $M = S$. The same procedure can be applied for the determination of the correct dipolar hyperfine coupling constants.

In the case of the strong exchange coupling limit, we have already demonstrated that our approach reduces to the treatment outlined by Bencini and Gatteschi.[32] Considering a dimer dominated by Heisenberg exchange, the on-site spin expectation value is related to the spin projection coefficient

$$C_A = \frac{\langle S_z^{(A)}\rangle}{S_t} \tag{6}$$

with

$$C_A = \frac{S_t(S_t+1)+S_A(S_A+1)-S_B(S_B+1)}{S_t(S_t+1)} \tag{7}$$

S_A and S_B being, respectively, the site spins of subsystems A and B in the dimer of interest. However, when Heisenberg exchange is not dominant the previous treatment is no longer valid, and we need to account for the zero-field splitting (ZFS) contribution that arises when at least one site has $S_i > {}^1/_2$. This can be done by simply including a new term in the effective spin-Hamiltonian of eq 3:

$$H_{\text{eff}} = -2\sum_{i<j} J_{ij}\hat{S}_i\cdot\hat{S}_j + \sum_i \hat{S}_i\cdot\tilde{D}^{(i)}\cdot\hat{S}_i \tag{8}$$

where $\tilde{D}^{(i)}$ is the local ZFS tensor for site *i*. By accounting for this term in our procedure, it is obvious that *S* is no longer a good quantum number. In extreme cases if either *J* is very small or *D* is very large this may well obscure the multiplet structure to an extent that the lowest magnetic sublevels can no longer be described by a standard spin-Hamiltonian. However, as long as the ground state multiplet remains a doublet upon inclusion of the ZFS interaction, it is still reasonable to describe the system of interest with $S_{\text{eff}} = S_t = {}^1/_2$ even though the ground state is not an eigenstate of $\hat{S}^2$. The calculation of the on-site spin expectation value is then performed by following eqs 3−5 for the general case of an exchange coupled system divided into metal-centered subsystems. This procedure allows us to extend our treatment of mixed-valence clusters into the intermediate exchange coupling regime and arrive at reliable predictions of HFCs for this case as well.

Geometry Optimization. Crystallographic files of the complexes were obtained from the Cambridge Structural Database. The experimental structures were processed and cleaned up to prepare the initial molecular geometries that were subsequently completed by addition and optimization of hydrogen atoms. These refined structures were fully optimized without symmetry restrictions to ensure that all complexes are treated on an equal footing and that subsequent spectroscopic properties are derived from a consistent set of reference structures. Geometry optimizations were performed with the BP86 functional[33,34] using TZVP basis sets for all atoms[35] and taking advantage of the RI approximation with the auxiliary def2-TZV/J Coulomb fitting basis sets[36] as implemented in ORCA.[37] Increased integration grids (Grid4 in ORCA convention) and tight SCF convergence criteria were used.

Magnetic properties. Broken-symmetry DFT calculations were performed with six different density functionals that represent most of the currently available approaches: the generalized gradient approximation (GGA) functionals BP86[33,34] and PBE,[38−40] the meta-GGA functional TPSS,[41] the hybrid functionals B3LYP[42−44] and PBE0,[45] and the hybrid meta-GGA functional TPSSh.[46] Exchange coupling constants were computed with the Yamaguchi formula[47,48] (eq 9) which

(32) Bencini, A.; Gatteschi, D. *EPR of Exchange Coupled Systems*; Springer Verlag: Berlin, 1990.

(33) Becke, A. D. *Phys. Rev. A* **1988**, *38*, 3098–3100.
(34) Perdew, J. P. *Phys. Rev. B* **1986**, *33*, 8822–8824.
(35) Schäfer, A.; Huber, C.; Ahlrichs, R. *J. Chem. Phys.* **1994**, *100*, 5829–5835.
(36) Weigend, A. *Phys. Chem. Chem. Phys.* **2006**, *8*, 1057–1065.
(37) Neese, F. *ORCA − an ab initio, Density Functional and Semiempirical Program Package* (*v. 2.6−35*); Universität Bonn: Bonn, Germany, 2007.
(38) Perdew, J. P.; Burke, K.; Ernzerhof, M. *Phys. Rev. Lett.* **1996**, *77*, 3865–3868.
(39) Perdew, J. P.; Burke, K.; Ernzerhof, M. *Phys. Rev. Lett.* **1997**, *78*, 1396–1396.
(40) Perdew, J. P.; Burke, K.; Wang, Y. *Phys. Rev. B* **1996**, *54*, 16533–16539.
(41) Tao, J.; Perdew, J. P.; Staroverov, V. N.; Scuseria, G. E. *Phys. Rev. Lett.* **2003**, *91*, 146401.
(42) Becke, A. D. *J. Chem. Phys.* **1993**, *98*, 5648–5652.
(43) Lee, C.; Yang, W.; Parr, R. G. *Phys. Rev. B* **1988**, *37*, 785–789.
(44) Hertwig, R. H.; Koch, W. *Chem. Phys. Lett.* **1997**, *268*, 345–351.
(45) Adamo, C.; Barone, V. *J. Chem. Phys.* **1999**, *110*, 6158–6170.
(46) Staroverov, V. N.; Scuseria, G. E.; Tao, J.; Perdew, J. P. *J. Chem. Phys.* **2003**, *119*, 12129–12137.
(47) Yamaguchi, K.; Takahara, Y.; Fueno, T. In *Applied Quantum Chemistry*; Smith, V. H., Jr., Schaefer, H. F., III, Morokuma, K., Eds.; D. Reidel: Boston, 1986; p 155.
(48) Yamanaka, S.; Kawakami, T.; Nagao, H.; Yamaguchi, K. *Chem. Phys. Lett.* **1994**, *231*, 25–33.

covers consistently the whole range of situations from the strong to the weak exchange coupling limit.

$$J = -\frac{E_{HS} - E_{BS}}{\langle \hat{S}^2 \rangle_{HS} - \langle \hat{S}^2 \rangle_{BS}} \quad (9)$$

Spectroscopic Parameters. ^{55}Mn isotropic hyperfine coupling constants A_{iso} and the traceless anisotropic dipolar HFCs were calculated from Fermi contact terms and dipolar contributions as the expectation values of the appropriate operators over the spin density. The spin−orbit contribution (orbital part) to the hyperfine interaction was also determined; its isotropic part (pseudocontact shift) was added to the ^{55}Mn isotropic Fermi contact term A_{iso}, while its anisotropic part was added to the anisotropic tensor. All HFC calculations were performed with ORCA using the TPSSh functional,[46] which has been identified as superior to other hybrid or GGA functionals for spectroscopic properties.[19,20] The CP(PPP) basis set was used for Mn[22] and TZVP basis sets[35] for the remaining atoms. As previously described, the increased flexibility of the triply polarized basis set CP(PPP) in the core region is expected to provide results close to the basis set limit for the isotropic contribution to the HFC.[22,49] To ensure the numerical accuracy of results the size of the integration grid was increased to 7 (ORCA convention) for the manganese atoms.[22] Additional hyperfine calculations were performed at the scalar relativistic level of theory using the zero-order regular approximation (ZORA) as implemented in ORCA.[50−52] In this case all basis sets were fully decontracted to allow for a more accurate response of the inner atomic shells to the relativistic potentials; the integration accuracy of the metal centers was also increased to 14.

Results and Discussion

Structures. The fourteen complexes under consideration are listed in Table 1, and their optimized structures are shown in Figure 1. As stressed in the Introduction, we attempted to be exhaustive but discriminating in our coverage of existing Mn(III/IV) dimers; thus, the lack of EPR studies and in particular HFCs for many otherwise characterized complexes led us to exclude them from the present reference set. For a detailed overview of the literature on manganese clusters we refer the reader to the comprehensive review by Armstrong and co-workers.[1] Focusing on the available dimers collected in Table 1, we note that the bridging motif of the dimanganese core is largely determined by the denticity of the supporting ligands. Thus, the use of a pentadentate N_4O-donor ligand in complex **1** results in a μ-oxo bridge featuring an almost perfectly linear Mn−O−Mn arrangement.[53] This is currently the only known example of a Mn(III/IV) dimer with a single μ-oxo bridge. Complexes **2**−**8** contain the more common bis(μ-oxo) core, while in complexes **9**−**13** the coordination sites that remain available through the use of either two tridentate or one hexadentate N-donor ligands accommodate an additional μ-carboxylato bridge. These 13 compounds cover the oxo/carboxylato bridging combinations that are most frequently encountered in biological settings. No mixed-valence Mn dimer is yet known with a (μ-oxo)-(μ-carboxylato) core; a Mn(III/IV) dimer featuring a (μ-oxo)bis(μ-carboxylato) core has been incompletely characterized,[54,55] while a dimer featuring bis(μ-oxo)bis-(μ-carboxylato) bridging has been reported by Mukhopadhyay and Armstrong,[56] but is not included in the present study because of the lack of detailed experimental data necessary for our purposes. The last compound in our set, dimer **14**, is a special case that cannot be classified into any of the usual core types: two hCl_2salpn ligands (hCl_2salpn = *N,N*′-bis(3,5-dichlorosalicylidene)-1,3-diamino-2-hydroxypropane) coordinate over both Mn centers, albeit with different ligation modes, leaving an alkoxy-group of one ligand to play the role of direct bridge between the manganese. This intriguing bonding situation leads to magnetic and spectroscopic properties that are atypical of the other Mn(III/IV) dimers, as will be discussed in the following.

In all cases, the computed spin densities of the complexes show clearly the inequivalent nature of the two manganese sites and the existence of discrete Mn(III) and Mn(IV) centers. A spin population of about 3.9 is assigned to the Mn(III) ion as anticipated for a high-spin d^4 center, whereas the Mn(IV) ion (d^3) carries a spin population of 2.7−2.8. The localized nature of these mixed-valence dimers is apparent in the optimized geometric parameters because of the high structural asymmetry that is present even when identical ligands are used for both metal ions. In particular, the Mn(III) center exhibits a large axial Jahn−Teller elongation, making the metal−ligand bonds involved 0.2−0.3 Å longer compared to the corresponding bonds of the Mn(IV) center. It should be noted that the Jahn−Teller axis is never found to lie along

(49) Neese, F. *J. Chem. Phys.* **2003**, *118*, 3939–3948.
(50) van Wüllen, C. *J. Chem. Phys.* **1998**, *109*, 392–399.
(51) van Lenthe, E.; Snijders, J. G.; Baerends, E. J. *J. Chem. Phys.* **1996**, *105*, 6505–6516.
(52) Pantazis, D. A.; Chen, X. Y.; Landis, C. R.; Neese, F. *J. Chem. Theory Comput.* **2008**, *4*, 908–919.
(53) Horner, O.; Anxolabéhère-Mallart, E.; Charlot, M. F.; Tchertanov, L.; Guilhem, J.; Mattioli, T. A.; Boussac, A.; Girerd, J. J. *Inorg. Chem.* **1999**, *38*, 1222–1232.
(54) Sheats, J. E.; Czernuszewicz, R. S.; Dismukes, G. C.; Rheingold, A. L.; Petrouleas, V.; Stubbe, J.; Armstrong, W. H.; Beer, R. H.; Lippard, S. J. *J. Am. Chem. Soc.* **1987**, *109*, 1435–1444.
(55) Zheng, M.; Khangulov, S. V.; Dismukes, G. C.; Barynin, V. V. *Inorg. Chem.* **1994**, *33*, 382–387.
(56) Mukhopadhyay, S.; Armstrong, W. H. *J. Am. Chem. Soc.* **2003**, *125*, 13010–13011.
(57) Jensen, A. F.; Su, Z.; Hansen, N. K.; Larsen, F. K. *Inorg. Chem.* **1995**, *34*, 4244–4252.
(58) Schäfer, K. O.; Bittl, R.; Zweygart, W.; Lendzian, F.; Haselhorst, G.; Weyhermüller, T.; Wieghardt, K.; Lubitz, W. *J. Am. Chem. Soc.* **1998**, *120*, 13104–13120.
(59) Manchanda, R.; Brudvig, G. W.; de Gala, S.; Crabtree, R. H. *Inorg. Chem.* **1994**, *33*, 5157–5160.
(60) Hureau, C.; Blondin, G.; Cesario, M.; Un, S. *J. Am. Chem. Soc.* **2003**, *125*, 11637–11645.
(61) Frapart, Y. M.; Boussac, A.; Albach, R.; Anxolabéhère-Mallart, E.; Delroisse, M.; Verlhac, J. B.; Blondin, G.; Girerd, J. J.; Guilhem, J.; Cesario, M.; Rutherford, A. W.; Lexa, D. *J. Am. Chem. Soc.* **1996**, *118*, 2669–2678.
(62) Horner, O.; Charlot, M.-F.; Boussac, A.; Anxolabéhère-Mallart, E.; Tchertanov, L.; Guilhem, J.; Girerd, J. J. *Eur. J. Inorg. Chem.* **1998**, *1998*, 721–727.
(63) Goodson, P. A.; Glerup, J.; Hodgson, D. J.; Michelsen, K.; Pedersen, E. *Inorg. Chem.* **1990**, *29*, 503–508.
(64) Hagen, K. S.; Armstrong, W. H.; Hope, H. *Inorg. Chem.* **1988**, *27*, 967–969.
(65) Suzuki, M.; Senda, H.; Kobayashi, Y.; Oshio, H.; Uehara, A. *Chem. Lett.* **1988**, 1763–1766.
(66) Wieghardt, K.; Bossek, U.; Zsolnai, L.; Huttner, G.; Blondin, G.; Girerd, J. J.; Babonneau, F. *J. Chem. Soc., Chem. Commun.* **1987**, 651–653.
(67) Pal, S.; Gohdes, J. W.; Wilisch, W. C. A.; Armstrong, W. H. *Inorg. Chem.* **1992**, *31*, 713–716.
(68) Pal, S.; Olmstead, M. M.; Armstrong, W. H. *Inorg. Chem.* **1995**, *34*, 4708–4715.
(69) Larson, E.; Haddy, A.; Kirk, M. L.; Sands, R. H.; Hatfield, W. E.; Pecoraro, V. L. *J. Am. Chem. Soc.* **1992**, *114*, 6263–6265.

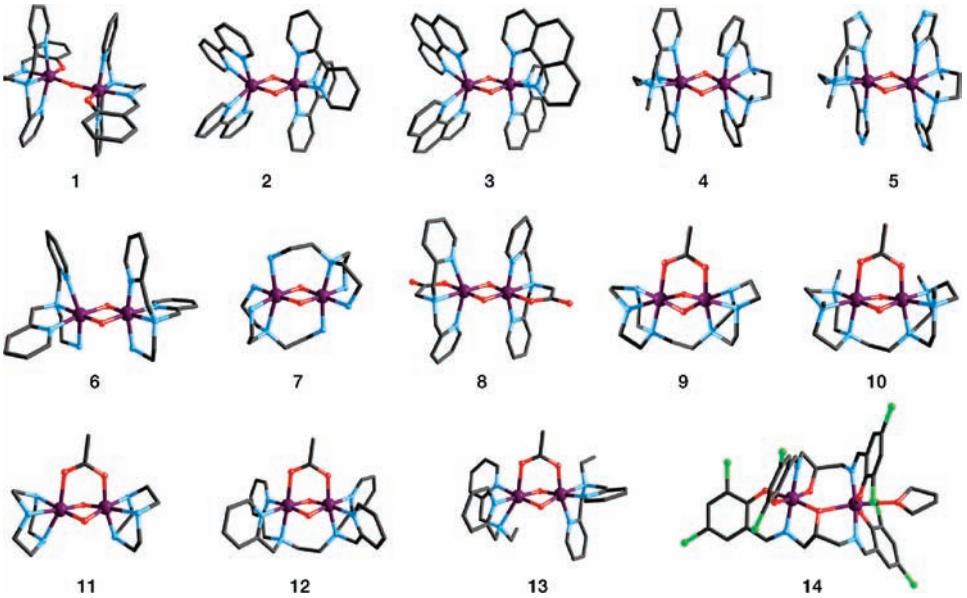

Figure 1. Optimized structures (BP86/TZVP) of the mixed-valence manganese(III/IV) dimers (hydrogen atoms omitted for clarity).

an oxo bridge. The equatorial bonds around Mn(III) are also longer than those of the Mn(IV) center, but to a smaller extent. In most cases, the equatorial elongation (usually less than 0.1 Å) is only noticeable in the bridging Mn−O bonds and not in the Mn−N bonds with the supporting ligands. Finally, we observe that geometric features such as the distance between the manganese centers are strictly defined for each particular type of bridging and can span only a very limited range of values. Specifically, complexes with the bis(μ-oxo) core (**2**−**8**) have an intermetallic distance between 2.75 and 2.76 Å, coinciding with the hallmark value for one of the EXAFS-derived Mn···Mn separations in the OEC.[70] The Mn_2O_2 moiety is perfectly planar and the Mn−O−Mn angles remain almost constant at 96° in all these dimers. The addition of a carboxylato bridge (complexes **9**−**13**) enforces a bending of the Mn_2O_2 ring along the O−O vector by ∼20° and reduces the distance between the metal centers to 2.66−2.69 Å. The Mn···Mn distance is significantly longer in complexes **1** and **14**, at 3.73 Å.

Heisenberg Exchange Coupling Constants. The values of the exchange coupling constants obtained with the six density functionals employed in this study are summarized in Table 2. Across the set, exchange coupling is uniformly predicted to be antiferromagnetic. The three functionals that do not include Hartree−Fock exchange (TPSS, BP86, and PBE) demonstrate the typical overestimation of the magnitude of the exchange coupling, arising from the overdelocalization that is characteristic of GGA functionals. BP86 and PBE show deviations in excess of 50%, whereas TPSS is slightly better, with average deviations of 43%. Incorporation of exact exchange in the hybrid functionals PBE0 and B3LYP leads to a clear improvement, reducing the deviation to 23% in the latter case. For the hybrid functionals the tendency is to underestimate the magnitude of the coupling constant, possibly in part because of overstabilization of the high-spin states by the Hartree−Fock contribution.[8] Overall, however, the hybrid meta-GGA TPSSh functional yields the best results, with absolute deviations of only 14%. These results reinforce the view emerging from a number of recent studies[19,20,71−74] that TPSSh outperforms B3LYP in many situations and should be considered as the method of choice especially for modeling magnetic and spectroscopic properties of exchange coupled transition metal clusters.

Table 2. Exchange Coupling Constants J (in cm^{-1}) Computed with Different Density Functionals: Comparison with Experimental Values

dimer	TPSSh	B3LYP	PBE0	TPSS	BP86	PBE	expt.
1	−120	−101	−85	−168	−185	−187	−177
2	−147	−123	−100	−218	−239	−242	−150
3	−147	−123	−100	−216	−237	−240	−134
4	−128	−109	−88	−189	−208	−210	−155
5	−127	−109	−89	−183	−201	−203	−139
6	−125	−106	−86	−183	−201	−203	−140
7	−127	−106	−83	−190	−208	−209	−146
8	−118	−100	−82	−172	−188	−190	−151
9	−138	−114	−96	−209	−230	−232	−110
10	−126	−105	−86	−193	−213	−215	−112
11	−118	−99	−81	−178	−196	−198	−110
12	−129	−106	−87	−197	−217	−219	−125
13	−107	−91	−75	−161	−179	−180	−164
14	−10	−7	−4	−18	−20	−20	−10
% ΔJ	−6	−22	−37	42	56	58	
% $\lvert\Delta J\rvert$	14	23	37	43	56	58	

When the computed values are looked at more closely, it is somewhat surprising that no clear trends and correlations appear between the J values and the bridging motifs of the dimers. The experimentally fitted constants suggest that the bis(μ-oxo) core corresponds, in general, to stronger antiferromagnetic coupling compared to the bis(μ-oxo)(μ-carboxylato) core. Dimer **13** constitutes an

(70) Yachandra, V. K.; Sauer, K.; Klein, M. P. *Chem. Rev.* **1996**, *96*, 2927–2950.

(71) Bühl, M.; Reimann, C.; Pantazis, D. A.; Bredow, T.; Neese, F. *J. Chem. Theory Comput.* **2008**, *4*, 1449–1459.

(72) Pantazis, D. A.; McGrady, J. E.; Maseras, F.; Etienne, M. *J. Chem. Theory Comput.* **2007**, *3*, 1329–1336.

(73) Bühl, M.; Kabrede, H. *J. Chem. Theory Comput.* **2006**, *2*, 1282–1290.

(74) Jensen, K. P. *Inorg. Chem.* **2008**, *47*, 10357–10365.

exception, since the reported J constant has the unusually high value of $-164\ cm^{-1}$. This trend is not at all apparent in the computed values, which are of comparable magnitude for complexes **2**−**8** and complexes **9**−**13**. Another distinctive feature in the experimental data that is not reproduced by the calculations is the magnitude of the coupling constant for **1**. According to the fitted J, this mono(μ-oxo) dimer was expected to display the strongest coupling, but this is clearly not the case with the DFT values. We attribute this particular deviation to the lengthening of the Mn(III)−O bond upon optimization by 0.13 Å with respect to the starting crystal structure. This elongation, which is to be expected for this type of linear bridging given the absence of packing constraints in our models, should be enough to cause the observed lowering in the absolute value of the exchange coupling constant. Indeed, recalculating the exchange coupling constant for **1** with the Mn−O distances fixed at their crystallographic values leads to $J = -215\ cm^{-1}$. This demonstrates the high sensitivity of the calculated J value toward changes in the Mn−O distance, which regulates the dominant σ superexchange pathway for **1**.

It is worth noting that the above observations are not specific to any functional: all of the approaches presented in Table 2 yield essentially the same relative magnitudes for the J constants of the different complexes. We will not pursue this issue here; in each individual case comparisons are inevitably complicated by a combination of ill-defined factors such as experimental uncertainties in the thermal depopulation measurements and/or the fitting procedure, the possible influence of counterions and crystal environment on geometries, intermolecular interactions and intrinsic errors of the theoretical methods. For our purposes, and for all practical purposes we can envisage, it is sufficient that we have singled out an adequately performing density functional (TPSSh) for the broken-symmetry description of these complexes, so we will now proceed to the analysis of the spectroscopic properties of the Mn(III/IV) dimers.

Manganese Hyperfine Tensors. In previous theoretical studies it has been shown that present-day density functionals tend to underestimate the ^{55}Mn isotropic hyperfine coupling constant because of the inadequate description of spin polarization.[49,75] The observed deviations turn out to be systematic and can be compensated by applying a universal scaling factor that is specific to a given combination of functional and basis set. In a calibration study that compared experimental and calculated ^{55}Mn isotropic HFCs for some representative mononuclear and binuclear manganese complexes a scaling factor of 1.59 was determined for the B3LYP functional using the CP(PPP) and TZVP basis sets for the metal and the remaining atoms, respectively.[21] Since we are employing a different functional (TPSSh) an updated scaling factor is necessary; the outcome of the new calibration is presented in Table 3. To test the influence of scalar relativistic effects we have also computed the isotropic hyperfine coupling constants of the above set of manganese complexes using the ZORA scalar relativistic Hamiltonian.

(75) Munzarová, M.; Kaupp, M. *J. Phys. Chem. A* **1999**, *103*, 9966–9983.

The results in Table 3 suggest a scaling factor of 1.49 for the non-relativistic TPSSh results. It is important to note that the values obtained for the dimer [$Mn^{III}Mn^{IV}$-(μ-O)2(μ-OAc)(dtne)]$^{2+}$ confirm that the same scaling factor also applies to metal centers involved in antiferromagnetic coupling, which is an important requisite for the present study. The ZORA results appear better, reducing the error roughly by half compared with the non-relativistic case. However, the hyperfine coupling constants are still underestimated on average by a factor of 1.24 with respect to the experimental values. Most importantly, the results are not more systematic than the non-relativistic results, since scalar relativistic corrections do not improve on the description of the bonding in the valence region. Therefore, given that the use of the ZORA approximation does not eliminate the need for a scaling factor and also tends to be slightly more time-consuming than the usual non-relativistic calculations, we consider it more convenient to pursue this work by applying a scaling factor on non-relativistic values. It simply should be kept in mind that the factor of 1.49 accounts in about 1:1 ratio for both spin polarization effects and scalar relativistic corrections.

Usually, with bridging ligands such as those encountered in the selected set of compounds, the ground state of a mixed-valence Mn(III,IV) dimer is an antiferromagnetically coupled doublet $S_t = {}^1/_2$ state, which can be described by the BS state $|2,-3/2\rangle$. Furthermore, the major part of the dimers under investigation is close to the strong exchange coupling limit according to the results reported in Table 2. It is thus straightforward to calculate the corresponding on-site spin expectations values by using eqs 6 and 7. For the present doublet systems, we calculated $\langle S_z^{(A)}\rangle = 1$ for the Mn(III) ions ($S_A = 1$) and $\langle S_z^{(B)}\rangle = -{}^1/_2$ for the Mn(IV) ions ($S_B = 3/2$). With these values in hand, we subsequently calculated the hyperfine coupling constants of the relevant BS state $A^{(K)}_{iso,BS}$. The conversion of these quantities into "site values" $A^{(K)}_{iso,site}$ and their multiplication with the corresponding $\langle S_z^{(K)}\rangle/S_t$ ratio finally provided the correct isotropic and anisotropic ^{55}Mn HFCs. The results are summarized in Tables 4 and 5, where the experimentally deduced parameters are also given for comparison.

Looking first at the anisotropic contributions to the HFCs (Table 4), our calculations confirm that the Mn(III) center is the main source of anisotropy for the entire set of complexes under investigation. The largest component is predicted to be along the z-axis, in agreement with available experimental data. This point is also consistent with the fact that all reduced sites in these dimers exhibit a Jahn−Teller distortion in the axial direction. Regarding now the magnitude of the computed dipolar HFCs, the A'_z values seem to be correctly predicted since most of them are in the range of the experimental data. However, the calculations clearly overestimate the values of the A'_x and A'_y components and it is also not clear whether they can reproduce the rhombic or the axial nature of the corresponding tensors. Nevertheless, it is worth bearing in mind that it is difficult to reach any safe conclusions regarding the performance of the method because the experimental data vary widely in terms of consistency and accuracy.

Table 3. Determination of a Scaling Factor f_{iso} for the Isotropic HFC: Comparison between Calculated (TPSSh) and Experimental Isotropic ^{55}Mn HFCs (MHz) of Selected Mn Complexes[a]

			NonRel		ZORA	
redox state	complex	A_{iso} (exp)	A_{iso} (calc)	f_{iso}	A_{iso} (calc)	f_{iso}
Mn^{II}	$[Mn(H_2O)^6]^{2+}$	−264	−201	1.31	−232	1.14
Mn^{II}	$[Mn(porph)(NH_3)_2]$	−204	−123	1.66	−147	1.39
Mn^{IV}	$[Mn(porph)(OCH_3)_2]$	−202	−139	1.45	−167	1.21
Mn^{IV}	$[Mn(salahe)_2]$	−216	−128	1.68	−154	1.40
Mn^{III}	$[Mn^{III}Mn^{IV}(\mu\text{-}O)_2(\mu\text{-}OAc)(dtne)]^{2+}$	−389	−278	1.40	−338	1.15
Mn^{IV}	$[Mn^{III}Mn^{IV}(\mu\text{-}O)_2(\mu\text{-}OAc)(dtne)]^{2+}$	207	142	1.46	178	1.17

[a] Ligand abbreviations: porph = porphyrine; salahe = salicylaldehydeimine-1-hydroxyethane; dtne = 1,2-bis(1,4,7-triazacyclonon-1-yl)ethane.

Table 4. Calculated (TPSSh) ^{55}Mn Hyperfine Parameters (MHz): Spin Projected Anisotropic HFCs for the Selected Mixed-Valence Complexes, Compared with Experiment

		Mn_A^{III}			Mn_B^{IV}		
		A'_x	A'_y	A'_z	A'_x	A'_y	A'_z
1	Calc.	+67	+39	−106	−1	−11	+12
	Expt.	+99	+9	−108	+3	+3	−6
2	Calc.	+50	+46	−96	+1	+4	5
	Expt.	+49	+27	−76	−9	−3	+12
3	Calc.	+51	+45	−96	+2	+5	−7
	Expt.	+50	+28	−78	−7	−4	+11
4	Calc.	+50	+46	−96	−5	−2	+7
	Expt.	+28	+28	−56	+4	+4	−8
5	Calc.	+50	+47	−97	0	+7	−7
	Expt.	+24	+24	−48	+1	+1	−2
6	Calc.	+43	+56	−99	−3	−5	+8
	Expt.	+67	+19	−86	−9	0	+9
7	Calc.	+47	+50	−97	−3	−3	+6
	Expt.	+22	+22	−44	0	0	0
8	Calc.	+75	+34	−110	−5	−6	+11
	Expt.	+20	+20	−40	0	0	0
9	Calc.	+55	+50	−105	+3	+5	−8
	Expt.	+15	+79	−94	+12	+4	−16
10	Calc.	+47	55	−101	+5	+2	−6
	Expt.	+15	+77	−92	+11	+6	−17
11	Calc.	+51	+50	−101	−1	−7	+8
	Expt.	+24	+71	−95	+6	+9	−15
12	Calc.	+52	+50	−102	+1	+3	−4
	Expt.						
13	Calc.	+53	+48	−101	−6	−2	+8
	Expt.						
14	Calc.	+54	+49	−103	+7	+1	−8
	Expt.						

Indeed, although all EPR experiments were at least performed on frozen solutions studied at low temperature with the use of 9 GHz (X-band) spectrometers, the simulations of the spectra were conducted at different levels of approximation. For complexes **2**−**4** and **9**−**11**, an elaborate multifrequency approach was employed with the use of extra high-field EPR experiments. The resulting spectra were then carefully analyzed for an accurate determination of hyperfine tensors allowing thus a direct comparison of these data with our calculations. For complexes **1** and **6** the X-band spectra were analyzed by a least-squares fit allowing for rhombic hyperfine tensors thus leading to an appropriate level of agreement between experiment and simulation. However, only axial tensors were employed for simulating the X-band spectra of complexes **5** and **7**−**8**, thus limiting the reliability of a comparison between theory and experiment. Finally, nothing can be said about complexes **12**−**14** since no simulated data is available for these systems. Most importantly for our purposes, from comparison of Tables 4 and 5, and in line with previous work,[19,21,30] the anisotropic components of the ^{55}Mn hyperfine tensors are at least three times smaller than their isotropic counterparts, which were all properly determined from the EPR experiments. Therefore, we will focus the rest of our analysis on the isotropic parameters for the selected manganese dimers. Note that the same complications arise in comparing the calculated g-tensors with experimental data (see Supporting Information).

Correct signs for all calculated isotropic HFCs are obtained with respect to the spin-up/spin-down population carried by each fragment. We observe that the Mn(III) ions are characterized by similar intrinsic site values for identical bridging topologies: −216 MHz on average for bis(μ-oxo) bridging (complexes **2**−**8**) and −204 MHz on average for bis(μ-oxo)(μ-carboxylato) bridging (complexes **9**−**13**). Interestingly, the situation is slightly different for the Mn(IV) ions, which seem to be less affected by the chemical nature of the bridge as they display a common $A_{iso,site}$ value of −213 MHz. Thus, this parameter for the Mn(IV) center is not sensitive to the bridging environment. Furthermore, the largest isotropic values are predicted to correspond to the Mn(III) sites, consistent with the EPR simulations. Finally, comparison of the calculated and experimental ^{55}Mn isotropic HFCs A_{iso} reveals very good agreement between theory and experiment with average absolute deviations of only 5% and 3% for the Mn(III) and Mn(IV) sites, respectively. The only unusually high deviation from experiment is observed for complex **13**, with the calculated isotropic HFCs underestimating the experimental values by 16% and 11% for the respective manganese ions. However, the experimental HFC values for this complex appear to be somewhat high when compared to its closely related analogue **12**. No detailed justification has been provided to rationalize the difference in experimentally deduced values between dimers **13** and **12**. Thus, we do not consider this deviation to be of great concern. Overall, the present results confirm the reliability of the procedure elaborated for extracting the isotropic HFCs from a BS solution in the strong exchange limit.

In the above discussion, the comparison of calculated and experimental isotropic HFCs has been focused on complexes **1**−**13**. We will now turn our attention to dimer **14**, which is a special case when compared to the other complexes in our set of selected dimers. Thus, this complex will benefit from a specific treatment that we will discuss in the following. At first, as shown in Table 4, we calculated the ^{55}Mn isotropic HFCs of this dimer by applying the same methodology we used for complexes

Table 5. Calculated (scaled TPSSh) ^{55}Mn Hyperfine Parameters (MHz): Site Values and Spin Projected Isotropic HFCs for the Selected Mixed-Valence Complexes, Compared with Experiment

	Mn_A^{III}				Mn_B^{IV}			
	$A_{iso,site}$	A_{iso} (calc)	$\|A_{iso}\|$ (exp)	ΔA_{iso}	$A_{iso,site}$	A_{iso} (calc)	$\|A_{iso}\|$ (exp)	ΔA_{iso}
1	−178	−356	381	25	−181	181	183	2
2	−235	−471	452	19	−213	213	219	6
3	−233	−465	451	14	−212	212	220	8
4	−217	−434	408	26	−214	214	230	16
5	−209	−417	456	39	−217	217	216	4
6	−201	−402	413	11	−212	212	218	6
7	−211	−422	428	6	−206	206	207	1
8	−203	−406	430	24	−214	215	210	5
9	−207	−414	391	23	−211	211	209	2
10	−206	−411	405	6	−212	212	210	2
11	−195	−389	388	1	−213	213	215	2
12	−208	−417	448	31	−213	213	224	11
13	−203	−407	482	76	−215	215	241	26
14	−146	−292	387	95	−197	197	308	111
MAE				23				7

1−**13**, assuming the case of the strong exchange limit. Our predictions clearly disagree with experiment, the calculated isotropic HFCs being drastically underestimated when compared to the experimental values. Such deviation was expected for this complex as it features a J value that is an order of magnitude smaller than the values obtained for other dimers. Thus, complex **14** actually corresponds to the case of intermediate exchange, and for that reason we have to account for the Zero Field Splitting (ZFS) interaction to predict the spectroscopic parameters of this system. In this respect, we will apply the procedure described in the theoretical section (eq 8). This will lead us to new values for the on-site spin expectation coefficients and will provide corrected isotropic HFCs that can be directly compared to experiment.

To illustrate the role of the ZFS term in the actual modeling of the hyperfine couplings, we have calculated the relevant quantities, that is, the on-site expectation values $\langle S_z^{(K)}\rangle$ and the isotropic hyperfine coupling constants $A_{iso}^{(K)}$ for different values of the D_i and J_{ij} parameters, using exact diagonalization of the spin-Hamiltonian defined in eq 8. For this purpose, we only considered the case of antiferromagnetic coupling ($J_{AB} \leq 0$), and we varied the J_{AB} parameter to cover the range of experimental data: $-5\ cm^{-1} \leq J_{AB} \leq -175\ cm^{-1}$. Then, we assumed that we could neglect the ZFS of the Mn(IV) ion, while we varied the local ZFS parameter D_A of the Mn(III) ion over a range of typical values: $-1\ cm^{-1} \leq D_A \leq -4\ cm^{-1}$.[21,76,77] Finally, the intrinsic site isotropic HFCs used for the analysis were the values previously determined from DFT calculations for complex **14**, that is, $A_{iso,site}^{(A)} = -146$ MHz for the Mn(III) ion and $A_{iso,site}^{(B)} = -197$ MHz for the Mn(IV) ion. The dependence of the two quantities under study on the D_A and J_{AB} values is illustrated graphically in Figure 2.

According to the results, the two parameters $\langle S_z^{(K)}\rangle$ and $A_{iso}^{(K)}$ depend strongly on the values of D_A when the exchange interaction is no longer dominant, that is, when approximately $|J_{AB}| \leq 75\ cm^{-1}$. In this situation, the parameters for the Mn_A^{III} and Mn_B^{IV} sites are particularly sensitive to the ZFS of the Mn(III) ion with variations of up to 200 MHz for the calculated $A_{iso}^{(K)}$. From these plots we can infer that a good agreement between theory and experiment would be obtained for dimer **14** by using $J_{AB} \approx -10\ cm^{-1}$ and a value of D_A between $-3\ cm^{-1}$ and $-4\ cm^{-1}$. In this case, the corresponding on-site spin expectation coefficients are $\langle S_z^{(K)}\rangle = 1.27$ and $\langle S_z^{(B)}\rangle = -0.77$ when $D_A = -3\ cm^{-1}$, and $\langle S_z^{(A)}\rangle = 1.35$ and $\langle S_z^{(B)}\rangle = -0.85$ when $D_A = -4\ cm^{-1}$. On the basis of these values we then calculated the ^{55}Mn isotropic HFCs that are reported in Table 6. For comparison, we also include the effective HFCs that would be obtained by using smaller values for D_A.

Comparison of the calculated isotropic HFCs A_{iso} with experiment shows that the average absolute deviation for model **14** becomes 4% and 8% for the Mn^{III} and Mn^{IV} sites, respectively. Thus, the present results confirm that our procedure can be reliably extended for predicting the spectroscopic features of a system being in the situation of intermediate exchange coupling. Furthermore, the main advantage of our approach is the use of a limited number of assumptions, since the calculation of the on-site spin expectation coefficients is performed in an exact way as long as upon inclusion of the ZFS term the ground spin state under investigation remains a doublet ($S_t = {}^1/_2$).

Conclusions

In the present work, we have presented a systematic evaluation of density functional approaches for the prediction of the leading magnetic and spectroscopic parameters that are accessible in mixed-valence Mn(III)−Mn(IV) dimers: the exchange coupling parameter as well as the isotropic ^{55}Mn hyperfine coupling parameters. Overall, broken-symmetry DFT is seen to provide fairly reasonable estimations of the investigated properties. The predicted structures are of the same quality as one is used for DFT calculations on monomeric transition metal complexes.

For the Heisenberg exchange, the results of this study clearly demonstrate that hybrid functionals are more accurate than GGA functionals. This is consistent with results available in the literature,[19,20] at least if the strong interaction

(76) Yano, J.; Sauer, K.; Girerd, J.-J.; Yachandra, V. K. *J. Am. Chem. Soc.* **2004**, *126*, 7486–7495.
(77) Peloquin, J. M.; Campbell, K. A.; Randall, D. W.; Evanchik, M. A.; Pecoraro, V. L.; Armstrong, W. H.; Britt, R. D. *J. Am. Chem. Soc.* **2000**, *122*, 10926–10942.

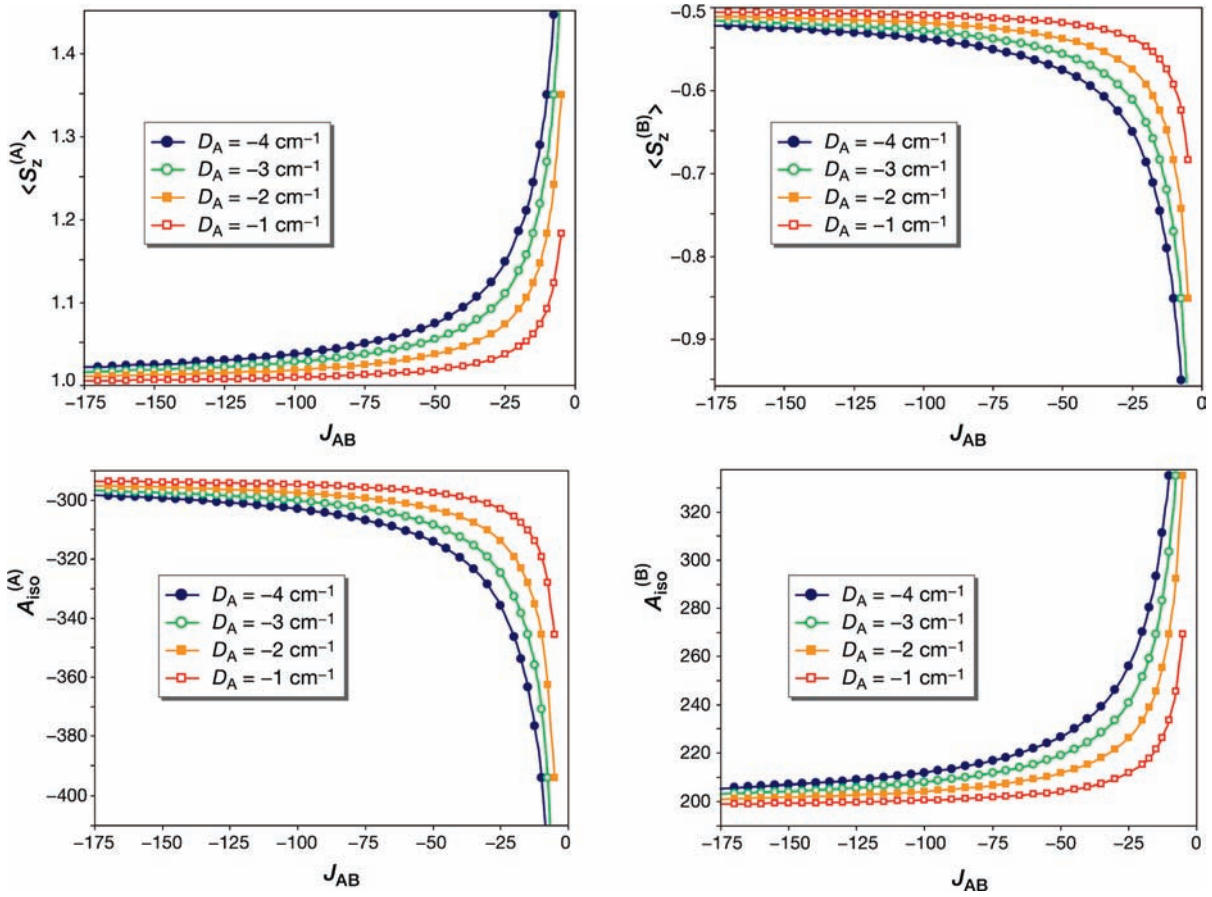

Figure 2. Calculated on-site spin expectation coefficients $\langle S_z^{(K)} \rangle$ and isotropic HFCs $A_{iso}^{(k)}$ as a function of the D_A and J_{AB} values.

Table 6. Comparison of Calculated (scaled TPSSh) and Experimental ^{55}Mn Hyperfine Data (MHz) for Dimer **14** for Different Values of the ZFS Parameter D_A

	Mn_A^{III}				Mn_B^{IV}			
D_A	$A_{iso,site}$	A_{iso} (calc)	$\lvert A_{iso}\rvert$ (exp)	ΔA_{iso}	$A_{iso,site}$	A_{iso} (calc)	$\lvert A_{iso}\rvert$ (exp)	ΔA_{iso}
0 cm^{-1}	−146	−292	387	95	−197	197	308	111
−1 cm^{-1}	−146	−319	387	68	−197	233	308	75
−2 cm^{-1}	−146	−346	387	41	−197	269	308	39
−3 cm^{-1}	−146	−371	387	16	−197	303	308	5
−4 cm^{-1}	−146	−394	387	7	−197	335	308	27

regime is assumed in the calculation of J values. It is pleasing to observe that the functional that has previously been identified as being the best one available for hyperfine predictions, the meta-GGA hybrid functional TPSSh, also turns out to deliver the best exchange coupling constants among all investigated methods. The deviations of theoretical and experimental J values are only on the order of ∼10−15% which is considered to be sufficient for most intents and purposes.

For the prediction of metal hyperfine couplings, it is still necessary to employ an empirical scaling factor that accounts for the shortcomings of DFT in the description of core-level spin-polarization. If scalar relativistic effects are taken into account (for example by the ZORA procedure), a deviation of 25% between theoretical and experimental ^{55}Mn HFCs still remains. However, this deviation is very systematic and can be essentially eliminated by one scaling factor that is once and for all fixed by a calibration study. It only depends on the functional and metal being investigated. However, if one does not want to deal with the intricacies of relativistic calculations, it is even easier to also compensate for the 25% scalar relativistic contribution to the isotropic ^{55}Mn hyperfine coupling with a combined scaling factor that turns out to be 1.49. Thus, this factor contains in equal proportions corrections due to the shortcomings of DFT and to the neglect of scalar relativistic effects.

Importantly, this scaling factor does not change upon coupling the manganese ions to antiferromagnetically coupled dimers. We expect that the same scaling factor will be valid for higher nuclearity clusters, although this remains to be proven in future studies. Thus, we have demonstrated that the ^{55}Mn hyperfine couplings in mixed valence Mn(III,IV) dimers can be successfully and systematically predicted with the TPSSh functional and the spin projection techniques that we have introduced earlier and that reduce to the Bencini−Gatteschi treatment in the case of dimers. This treatment is sound, simple, and successful as long as one is on the strong exchange limit. If, however, the exchange coupling becomes weak or the zero-field splitting (essentially dominated by the Mn(III) sites) becomes strong, the strong-exchange approximation breaks

down and then it becomes essential to employ a rigorous form of our spin projection technique that takes care of the ZFS contributions to the site spin-expectation values. In this study, we have demonstrated in one particular example that if the magnitude of the J value drops below 75 cm^{-1} the isotropic ^{55}Mn hyperfine couplings are very strongly affected by Mn(III) D values on the order of -3 to -4 cm^{-1}. This is an important result for future studies that aim at deducing unknown structures on the basis of computed spectroscopic parameters.

Having now a carefully calibrated DFT approach for Mn dimers available, we believe that the door is open for studying higher nuclearity manganese clusters and complex biochemical systems. Work along these lines is in progress in our laboratory.

Acknowledgment. We gratefully acknowledge financial support from the DFG priority program 1137 "Molecular Magnetism", from the EU (SOLAR-H2), from the University of Bonn and from the Max Planck Society.

Supporting Information Available: Cartesian coordinates of optimized structures and g-values. This material is available free of charge via the Internet at http://pubs.acs.org.